Avoided Quantum Criticality and Magnetoelastic Coupling in $BaFe_{2-x}Ni_xAs_2$

Xingye Lu,[1,2] H. Gretarsson,[3] Rui Zhang,[1] Xuerong Liu,[1,4] Huiqian Luo,[1] Wei Tian,[5] Mark Laver,[6,7] Z. Yamani,[8] Young-June Kim,[3] A. H. Nevidomskyy,[9] Qimiao Si,[9] and Pengcheng Dai[2,1,*]

[1]*Beijing National Laboratory for Condensed Matter Physics, Institute of Physics, Chinese Academy of Sciences, Beijing 100190, China*
[2]*Department of Physics and Astronomy, The University of Tennessee, Knoxville, Tennessee 37996-1200, USA*
[3]*Department of Physics, University of Toronto, 60 Saint George Street, Toronto, Ontario M5S 1A7, Canada*
[4]*Condensed Matter Physics and Materials Science Department, Brookhaven National Laboratory, Upton, New York 11973, USA*
[5]*Quantum Condensed Matter Division, Oak Ridge National Laboratory, Oak Ridge, Tennessee 37831, USA*
[6]*Laboratory for Neutron Scattering, Paul Scherrer Institute, CH-5232 Villigen, Switzerland*
[7]*Department of Physics, Technical University of Denmark, DK-2800 Kongens Lyngby, Denmark*
[8]*Canadian Neutron Beam Centre, National Research Council, Chalk River, Ontario K0J 1P0, Canada*
[9]*Department of Physics and Astronomy, Rice University, Houston, Texas 77005, USA*

(Received 29 March 2013; published 18 June 2013)

We study the structural and magnetic orders in electron-doped $BaFe_{2-x}Ni_xAs_2$ by high-resolution synchrotron x-ray and neutron scatterings. Upon Ni doping x, the nearly simultaneous tetragonal-to-orthorhombic structural (T_s) and antiferromagnetic (T_N) phase transitions in $BaFe_2As_2$ are gradually suppressed and separated, resulting in $T_s > T_N$ with increasing x, as was previously observed. However, the temperature separation between T_s and T_N decreases with increasing x for $x \geq 0.065$, tending toward a quantum bicritical point near optimal superconductivity at $x \approx 0.1$. The zero-temperature transition is preempted by the formation of a secondary incommensurate magnetic phase in the region $0.088 \lesssim x \lesssim 0.104$, resulting in a finite value of $T_N \approx T_c + 10$ K above the superconducting dome around $x \approx 0.1$. Our results imply an avoided quantum critical point, which is expected to strongly influence the properties of both the normal and superconducting states.

DOI: 10.1103/PhysRevLett.110.257001 PACS numbers: 74.70.Xa, 75.30.Gw, 78.70.Nx

A determination of the structural and magnetic phase diagram in correlated electron materials is important for understanding their underlying electronic excitations. In the iron pnictides, superconductivity arises at the border of both antiferromagnetic (AF) and structural orders [1–5]. This motivates the exploration of quantum critical points, where the transition temperatures for such orders are continuously suppressed to zero by a nonthermal control parameter. For the iron pnictide superconductors derived from electron or hole doping of their parent compounds, the most heavily studied materials are probably the electron-doped $BaFe_{2-x}T_xAs_2$ (where T = Co, Ni) because of the availability of high-quality single crystals [6–18]. In the undoped state, $BaFe_2As_2$ exhibits a tetragonal-to-orthorhombic structural transition at temperature T_s, and an AF phase transitions below nearly the same temperature $T_N \approx T_s \approx 138$ K [3,4]. Upon electron doping of $BaFe_2As_2$ via partially replacing Fe by Co or Ni, various experiments, including transport [8,9], neutron [11–16], and high-resolution x-ray scattering [4,18], reveal that the structural (T_s) and magnetic (T_N) phase transition temperatures in $BaFe_{2-x}T_xAs_2$ gradually decrease and separate with increasing x and have $T_s > T_N$ for all doping levels. In the initial x-ray [10] and neutron [11] scattering work on $BaFe_{2-x}Co_xAs_2$, it was suggested that the separated T_s and T_N smoothly extend into the superconducting dome, resulting in distinct structural and magnetic quantum critical points at different x. Subsequent x-ray [18] and neutron [12–14] scattering experiments on superconducting $BaFe_{2-x}T_xAs_2$ samples with coexisting AF order revealed that superconductivity actually competes with the static AF order and lattice orthorhombicity. As a consequence, the smoothly decreasing T_s and T_N are reported to bend back below T_c, and the orthorhombic structure above T_c for an optimally doped sample evolves back to a tetragonal structure well below T_c (termed the "reentrant" tetragonal phase) [18].

Although previous neutron [11–13] and x-ray diffraction [18] experiments have established the magnetic and structural phase transitions in $BaFe_{2-x}Co_xAs_2$, similar measurements have not been carried out on $BaFe_{2-x}Ni_xAs_2$. In this Letter, we describe neutron and x-ray scattering studies of structural and magnetic phase transitions in $BaFe_{2-x}Ni_xAs_2$, focusing on materials near optimal superconductivity [Fig. 1(a)]. While neutron scattering experiments on $BaFe_{2-x}T_xAs_2$ revealed a commensurate-to-incommensurate AF phase transition near optimal superconductivity [15–17], much remains unknown about the temperature and doping evolution of the orthorhombic lattice distortion for samples with an incommensurate AF order. Here, we find that $T_s > T_N$ for samples with commensurate AF order ($x \leq 0.065$), similar to the earlier results on $BaFe_{2-x}Co_xAs_2$ [11–13,18]. However, T_s and T_N tend to reconverge for larger values of x: $T_s - T_N$

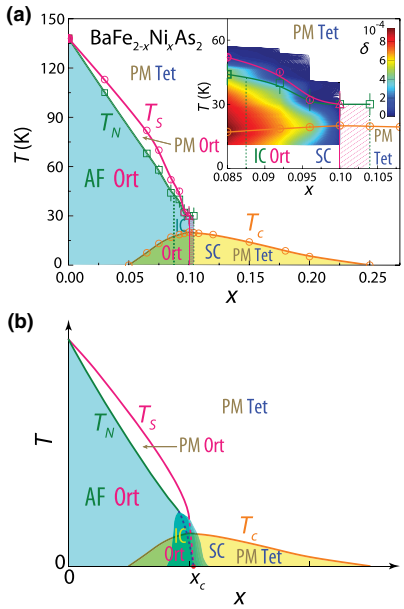

FIG. 1 (color online). (a) Electronic phase diagram of $BaFe_{2-x}Ni_xAs_2$ as a function of Ni doping x as determined from our neutron and x-ray scattering experiments. The PM Tet, PM Ort, AF Ort, and IC Ort are paramagnetic tetragonal, paramagnetic orthorhombic, commensurate AF orthorhombic, and incommensurate AF orthorhombic phases, respectively. The AF Ort, IC Ort, and PM Tet structures in the superconducting (SC) phase are clearly marked. The inset shows the expanded view of T_s, T_N, and T_c and temperature dependence of the orthorhombic lattice distortion order parameter $\delta = (a_o - b_o)/(a_o + b_o)$. The dashed region in the inset indicates the presence of a single Gaussian structural peak. (b) Schematic theoretical phase diagram for an avoided quantum bicritical point.

decreases for $x > 0.065$. This implicates a quantum bicritical point at $T = 0$, which is interrupted by a secondary short-range incommensurate AF order with a very small ordered moment [16]. The resulting overall phase diagram is illustrated schematically in Fig. 1(b). Our results are important to clarifying the nature of the purported quantum critical point in the carrier-doped iron pnictides, as inferred from the NMR [19,20], thermoelectric [21], and ultrasonic [22] measurements, as well as its connection with the quantum critical point of the isoelectronically tuned iron pnictides that was predicted by theory [23] and observed by extensive experiments [24,25].

We have carried out neutron scattering experiments on $BaFe_{2-x}Ni_xAs_2$ with $x = 0.085$, 0.092, 0.096, 0.1, 0.104 and 0.108 using the RITA-II cold neutron triple-axis spectrometer at the Paul-Scherrer Institute; the HB-1A thermal triple-axis spectrometer at the High-Flux Isotope Reactor, Oak Ridge National Laboratory; and the C5 triple-axis spectrometer at the Canadian Neutron Beam Centre, Chalk River Laboratories [26]. We have also performed high-resolution synchrotron x-ray diffraction experiments on identical $BaFe_{2-x}Ni_xAs_2$ samples using beam line X22C at the National Synchrotron Light Source, Brookhaven National Laboratory. The details of the experimental procedure are given in the Supplemental Material [27]. Although neutron scattering probes the bulk sample, whereas the length scale for x-ray diffraction is typically about ~5 micron [28], both techniques are measuring the intrinsic properties of these materials.

We first describe the determination of the Néel temperatures for $BaFe_{2-x}Ni_xAs_2$ using neutron scattering. Figure 2(a) shows transverse scans along the [1, K, 3] direction at different temperatures for the $x = 0.085$ sample. Consistent with earlier results [16], a well-defined commensurate AF order appears below 44 K. Figure 2(b) shows temperature dependence of the magnetic order parameter. Again, consistent with earlier results [15–17], the AF order appears approximately below $T_N = 44 \pm 5$ K and is suppressed from the onset of T_c. Figure 2(c) plots similar data for $x = 0.092$ and 0.096, showing $T_N = 40 \pm 5$ and 32 ± 5 K, respectively [16]. In the previous work on optimally

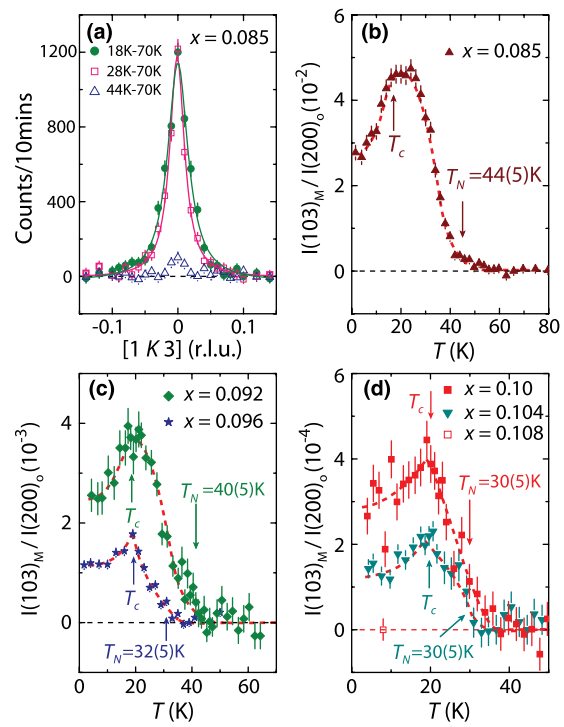

FIG. 2 (color online). (a) Transverse scans along the [1, K, 3] direction at different temperatures for $BaFe_{2-x}Ni_xAs_2$ with $x = 0.085$. The magnetic scattering of each temperature was obtained by subtracting the $T = 70$ K data as background. The change of the peak width between 18 and 28 K indicates the emergence of the short-range incommensurate AF order. Temperature dependence of the AF (1, 0, 3) peak normalized to the weak $(2, 0, 0)_o$ nuclear Bragg peak intensity for (b) $x = 0.085$, (c) $x = 0.092$ and 0.096, and (d) $x = 0.1$, 0.104, and 0.108. The T_N's and T_c's are marked by vertical arrows. Although there are two orders of magnitude magnetic scattering intensity reductions from $x = 0.085$ to 0.0104, the T_N's of the materials only decrease from $T_N = 44 \pm 5$ K to 30 ± 5 K. The data at 7 K for $x = 0.108$ were obtained by subtracting 50 K data as background.

electron-doped $BaFe_{1.9}Ni_{0.1}As_2$ [29], it was suggested, based on cold neutron data on mosaic crystals (~ 0.6 g) counting 1 min/point, that there is no measurable static AF order. Our new measurements on the $x = 0.1$ sample (~ 0.34 g) with much longer counting time (30 min/point on HB-1A) reveal a weak static AF order with magnetic scattering 5 times smaller than that of $x = 0.096$ [Figs. 2(c) and 2(d)]. Similar measurements on $x = 0.104$ also show the presence of a weak static AF order, which is 50% smaller than that of the $x = 0.1$ sample. In spite of their small moments, the temperature dependence of the magnetic order parameters for both samples indicates that their Néel temperatures are essentially unchanged at $T_N = 30 \pm 5$ K [Fig. 2(d)]. Finally, we find no evidence of static AF order for a $x = 0.108$ sample (~ 0.5 g) by counting 40 min/point on C5 [Fig. 2(d)].

In order to compare the onset of orthorhombicity with antiferromagnetism, high-resolution x-ray scattering measurements were performed on the samples identical to those used for neutron scattering. In all cases, we carried out longitudinal scans along the [H, 0, 12] direction. Figure 3(a) shows the outcome for $x = 0.085$, which has a superconducting $T_c = 16.5$ K. At $T = 58$ K, a temperature well above T_s, we see a single instrumentation resolution-limited peak, consistent with a tetragonal lattice. On cooling to $T = 45$, 30, and 17 K, the single peak

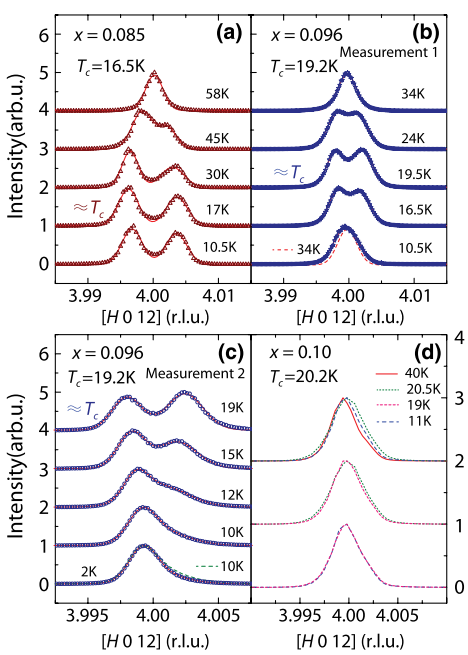

FIG. 3 (color online). Temperature evolution of the orthorhombic (4, 0, 12) and (0, 4, 12) Bragg peaks for $BaFe_{2-x}Ni_xAs_2$. Data in (a) are for $x = 0.085$, (b) $x = 0.096$ down to 10 K, (c) $x = 0.096$ down to 2 K, and (d) $x = 0.1$ where one can only see peak broadening due to orthorhombic lattice distortion. These measurements were performed with $E_i = 10$ keV synchrotron x-ray. The data were collected while warming the system from the base temperature to a temperature well above T_s.

splits into two peaks with increasing peak separations as temperature decreases down to T_c. Upon further cooling below T_c, the peak separations become smaller, as if the system turns back toward the tetragonal structure [18]. Figure 3(b) shows similar temperature-dependent scans for $x = 0.096$. Although the split peaks appear to become a single peak at $T = 10.5$ K, its width is still larger than that in the tetragonal phase ($T = 34$ K), suggesting that the nearly optimal superconductor has an orthorhombic lattice distortion at $T = 10.5$ K. To see how such orthorhombic lattice distortion evolves at lower temperatures, we carried out additional measurements using a cryostat capable of going down to 2 K. The longitudinal [H, 0, 12] scans in Fig. 3(c) show broad peaks at temperatures below 10 K, suggesting the presence of an orthorhombic lattice structure even at 2 K.

To quantitatively analyze the temperature dependence of the orthorhombic lattice distortion, we define lattice orthorhombicity $\delta = (a_o - b_o)/(a_o + b_o)$, where a_o and b_o are lattice parameters of the orthorhombic unit cell [18]. Figure 4(a) shows the temperature dependence of δ for $BaFe_{2-x}Ni_xAs_2$ with $x = 0.075$, 0.085, 0.092, 0.096, and 0.1. Figures 4(b) and 4(c) compare the ordered moment squared M^2 with the lattice orthorhombicity δ, and their similar temperature dependence suggests a strong magnetoelastic coupling.

The optimally doped $x = 0.1$ sample ($T_c = 20.2$ K) deserves special attention. Its temperature-dependent [H, 0, 12] scans are shown in Fig. 3(d). Although we can no longer see the double peaks, we observe a peak broadening that does not disappear at low temperatures. We therefore used the FWHM of the peak in order to determine the lattice orthorhombicity δ, similar to the analysis of $BaFe_{2-x}Co_xAs_2$ by Nandi *et al.* [18]. The deduced temperature dependence of δ is shown in Fig. 4(a) with red squares and appears to have a sharp cusp near the superconducting T_c. We conjecture that this cusp occurs because the electron-lattice coupling results in a lattice response to the superconducting fluctuations near T_c. At the lowest temperature measured $T = 11$ K, the value of δ is too small (2×10^{-5}) in order to unambiguously claim the orthorhombicity. However, taken together with magnetization squared for incommensurate AF order [see Fig. 4(c), which has a similar temperature dependence], we conclude that a weak static AF order likely coexists with orthorhombic lattice distortion in the optimally superconducting $BaFe_{2-x}Ni_xAs_2$, different from the reentrant tetragonal transition seen in $BaFe_{2-x}Co_xAs_2$ [18].

Figure 4(d) shows the Ni-doping dependence of δ and the ordered moment squared M^2, while Fig. 4(e) compares the doping dependence of δ in $BaFe_{2-x}Ni_xAs_2$ and in the previously reported $BaFe_{2-x}Co_xAs_2$ [18]. The essentially continuous suppression of both M^2 and δ near $x = 0.1$ provides further evidence for an extrapolated quantum critical point. For the magnetic ordering, this represents

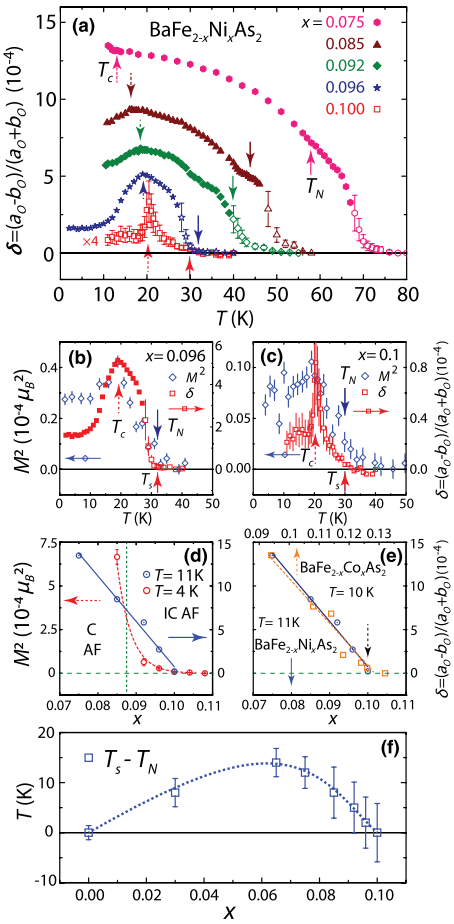

FIG. 4 (color online). (a) Orthorhombic lattice distortion δ as a function of temperature for $BaFe_{2-x}Ni_xAs_2$. The data denoted by the filled symbols are derived from fitting (4, 0, 12) and (0, 4, 12) Bragg peaks by two peaks, while the open symbols are data obtained from deconvolving the instrumental resolution-limited peak at a temperature above T_s. The magnitude of δ for $x = 0.1$ was multiplied by a factor of 4 for clarity. The vertical arrows indicate positions of T_N and T_c. Comparison of the temperature dependence of the magnetic order parameter and orthorhombic lattice distortion δ for (b) $x = 0.096$ and (c) $x = 0.1$. (d) Ni-doping dependence of the magnetic Bragg peak intensity at 11 K and δ. The vertical dashed line indicates the boundary between commensurate and incommensurate AF order. (e) Comparison of the Co- and Ni-doping [18] dependence of δ. In both cases, we see a structural quantum critical point near optimal superconductivity at $x=0.1$. (f) Electron-doping dependence of $T_s - T_N$.

a new understanding. On the other hand, for the orthorhombic distortion, the continuous suppression of δ with doping was already anticipated by ultrasound spectroscopy measurements [22,30].

Theoretically, this can be considered through a Landau-Ginzburg action for such a criticality, $S = S_M[\mathbf{M}] + S_{\mathrm{lat}}[\phi] + S_{\mathrm{lat}-M}[\mathbf{M}, \phi]$; the three terms, describing the magnetic and lattice parts, respectively, and their coupling, are given in the Supplemental Material [27]. This model resembles the previously studied $O(3) \times Z_2$ model [23], except that here the lattice quantum field ϕ is endowed with its own dynamics and undergoes Landau damping Γ_s, making it inherently quantum critical with the dynamic exponent $z = 3$. In two spatial dimensions, $d + z = 5$ for the ϕ field and $d + z = 4$ for the $\mathbf{M}$ fields. Because they are above or at the upper critical dimension, a quantum *bicritical* point for both orders is expected in the presence of the magnetoelastic coupling η. This is similar to the result of the $O(3) \times Z_2$ model [23] and is indicated schematically in Fig. 1(b). Indeed, as noted above, our measurements find that T_N and T_s get closer to each other as the quantum critical point is approached [see Figs. 1(a) and 4(f)] and the two order parameters disappear at the same point [Fig. 4(d)]. However, the appearance of an emergent incommensurate magnetism at $x \approx 0.088$ severely reduces the scattering rate γ and Γ_s (in addition to modifying other parameters of the effective theory), thereby eliminating the quantum critical point. A quantum critical point preempted by an emergent order is often referred to as "avoided" quantum criticality [31–33].

From direct measurements of the order parameters for both the AF and structural transitions, our results provide a solid basis for quantum criticality in carrier-doped iron pnictides, which has so far been indirectly deduced from the temperature dependences of magnetic, transport, or acoustic properties [19–22]. In addition, because the primary AF order in the electron-doped iron pnictides discussed here is commensurate, our results suggest that the quantum critical point arising under the carrier doping is surprisingly similar to that induced by isoelectronic doping [23–25]; the main distinction of the carrier doping is to introduce a secondary incommensurate order. This reveals an important universality of the underlying physics for the iron pnictides under carrier and isoelectronic dopings.

Summarizing the results presented in Figs. 2–4, we show in Fig. 1(a) the refined phase diagram of $BaFe_{2-x}Ni_xAs_2$, in agreement with the theoretically expected one [Fig. 1(b)]. While the phase diagram is mostly consistent with the earlier work on $BaFe_{2-x}Co_xAs_2$ at low electron-doping levels [18], our key new finding is that when x approaches optimal doping, the magnetic and structural transition temperatures converge to the purported quantum bicritical point, with both order parameters disappearing near $x \approx 0.1$ [Fig. 4(d)] as a result of magnetoelastic coupling. However, the emergent short-range incommensurate magnetism helps the system avoid the quantum critical fate, resulting in an apparent saturation of $T_s \sim T_N \approx 30$ K above the superconducting T_c near optimal doping $x = 0.1$, as shown in Fig. 1(a). These results elucidate the quantum criticality in the carrier-doped iron pnictides and its connection with that of the isoelectronically doped counterparts, and reveal a rich theoretical picture that should be further explored in future work.

The work at IOP, CAS, is supported by MOST (973 Projects No. 2012CB821400 and No. 2011CBA00110) and

NSFC (No. 11004233). The work at UTK is supported by the U.S. NSF-DMR-1063866. The work at Rice University is supported by the U.S. NSF-DMR-1006985 and the Robert A. Welch Foundation Grants No. C-1411 and No C-1818. Research at the University of Toronto was supported by the NSERC and CFI. Use of the NSLS was supported by the U.S. DOE, BES, under Contract No. DE-AC02-98CH10886. The work at the HFIR, ORNL, was sponsored by the Scientific User Facilities Division, BES, U.S. DOE.

*pdai@utk.edu

[1] Y. Kamihara, T. Watanabe, M. Hirano, and H. Hosono, J. Am. Chem. Soc. **130**, 3296 (2008).
[2] C. de la Cruz *et al.*, Nature (London) **453**, 899 (2008).
[3] Q. Huang, Y. Qiu, W. Bao, M. A. Green, J. W. Lynn, Y. C. Gasparovic, T. Wu, G. Wu, and X. H. Chen, Phys. Rev. Lett. **101**, 257003 (2008).
[4] M. G. Kim, R. M. Fernandes, A. Kreyssig, J. W. Kim, A. Thaler, S. L. Bud'ko, P. C. Canfield, R. J. McQueeney, J. Schmalian, and A. I. Goldman, Phys. Rev. B **83**, 134522 (2011).
[5] P. Dai, J. P. Hu, and E. Dagotto, Nat. Phys. **8**, 709 (2012).
[6] A. S. Sefat, R. Jin, M. A. McGuire, B. C. Sales, D. J. Singh, and D. Mandrus, Phys. Rev. Lett. **101**, 117004 (2008).
[7] L. J. Li, Y. K. Luo, Q. B. Wang, H. Chen, Z. Ren, Q. Tao, Y. K. Li, X. Lin, M. He, Z. W. Zhu, G. H. Cao, and Z. A. Xu, New J. Phys. **11**, 025008 (2009).
[8] N. Ni, M. E. Tillman, J.-Q. Yan, A. Kracher, S. T. Hannahs, S. L. Bud'ko, and P. C. Canfield, Phys. Rev. B **78**, 214515 (2008).
[9] J.-H. Chu, J. G. Analytis, C. Kucharczyk, and I. R. Fisher, Phys. Rev. B **79**, 014506 (2009).
[10] R. Prozorov, M. A. Tanatar, N. Ni, A. Kreyssig, S. Nandi, S. L. Bud'ko, A. I. Goldman, and P. C. Canfield, Phys. Rev. B **80**, 174517 (2009).
[11] C. Lester, J.-H. Chu, J. G. Analytis, S. C. Capelli, A. S. Erickson, C. L. Condron, M. F. Toney, I. R. Fisher, and S. M. Hayden, Phys. Rev. B **79**, 144523 (2009).
[12] D. K. Pratt, W. Tian, A. Kreyssig, J. L. Zarestky, S. Nandi, N. Ni, S. L. Bud'ko, P. C. Canfield, A. I. Goldman, and R. J. McQueeney, Phys. Rev. Lett. **103**, 087001 (2009).
[13] A. D. Christianson, M. D. Lumsden, S. E. Nagler, G. J. MacDougall, M. A. McGuire, A. S. Sefat, R. Jin, B. C. Sales, and D. Mandrus, Phys. Rev. Lett. **103**, 087002 (2009).
[14] M. Y. Wang, H. Q. Luo, M. Wang, S. Chi, J. A. Rodriguez-Rivera, D. Singh, S. Chang, J. W. Lynn, and P. Dai, Phys. Rev. B **83**, 094516 (2011).
[15] D. K. Pratt, M. G. Kim, A. Kreyssig, Y. B. Lee, G. S. Tucker, A. Thaler, W. Tian, J. L. Zarestky, S. L. Bud'ko, P. C. Canfield, B. N. Harmon, A. I. Goldman, and R. J. McQueeney, Phys. Rev. Lett. **106**, 257001 (2011).
[16] H. Q. Luo, R. Zhang, M. Laver, Z. Yamani, M. Wang, X. Y. Lu, M. Y. Wang, Y. C. Chen, S. L. Li, S. Chang, J. W. Lynn, and P. Dai, Phys. Rev. Lett. **108**, 247002 (2012).
[17] M. G. Kim, J. Lamsal, T. W. Heitmann, G. S. Tucker, D. K. Pratt, S. N. Khan, Y. B. Lee, A. Alam, A. Thaler, N. Ni, S. Ran, S. L. Bud'ko, K. J. Marty, M. D. Lumsden, P. C. Canfield, B. N. Harmon, D. D. Johnson, A. Kreyssig, R. J. McQueeney, and A. I. Goldman, Phys. Rev. Lett. **109**, 167003 (2012).
[18] S. Nandi, M. G. Kim, A. Kreyssig, R. M. Fernandes, D. K. Pratt, A. Thaler, N. Ni, S. L. Bud'ko, P. C. Canfield, J. Schmalian, R. J. McQueeney, and A. I. Goldman, Phys. Rev. Lett. **104**, 057006 (2010).
[19] F. L. Ning, K. Ahilan, T. Imai, A. S. Sefat, R. Jin, M. A. McGuire, B. C. Sales, and D. Mandrus, J. Phys. Soc. Jpn. **78**, 013711 (2009).
[20] F. L. Ning, K. Ahilan, T. Imai, A. S. Sefat, M. A. McGuire, B. C. Sales, D. Mandrus, P. Cheng, B. Shen, and H.-H Wen, Phys. Rev. Lett. **104**, 037001 (2010).
[21] M. Gooch, B. Lv, B. Lorenz, A. M. Guloy, and C.-W. Chu, Phys. Rev. B **79**, 104504 (2009).
[22] M. Yoshizawa, D. Kimura, T. Chiba, S. Simayi, Y. Nakanishi, K. Kihou, C.-H. Lee, A. Iyo, H. Eisaki, M. Nakajima, and S. Uchida, J. Phys. Soc. Jpn. **81**, 024604 (2012).
[23] J. Dai, Q. Si, J.-X. Zhu, and E. Abrahams, Proc. Natl. Acad. Sci. U.S.A. **106**, 4118 (2009).
[24] C. de la Cruz, W. Z. Hu, S. Li, Q. Huang, J. W. Lynn, M. A. Green, G. F. Chen, N. L. Wang, H. A. Mook, Q. Si, and P. Dai, Phys. Rev. Lett. **104**, 017204 (2010).
[25] S. Kasahara, T. Shibauchi, K. Hashimoto, K. Ikada, S. Tonegawa, R. Okazaki, H. Shishido, H. Ikeda, H. Takeya, K. Hirata, T. Terashima, and Y. Matsuda, Phys. Rev. B **81**, 184519 (2010).
[26] H. Q. Luo, Z. Yamani, Y. C. Chen, X. Y. Lu, M. Wang, S. L. Li, T. A. Maier, S. Danilkin, D. T. Adroja, and P. Dai, Phys. Rev. B **86**, 024508 (2012).
[27] See Supplemental Material at http://link.aps.org/supplemental/10.1103/PhysRevLett.110.257001 for a detailed discussion on the experimental setup and theory.
[28] U. Rütt, A. Diederrichs, J. R. Schneider, and G. Shirane, Europhys. Lett. **39**, 395 (1997).
[29] S. Chi, A. Schneidewind, J. Zhao, L. W. Harriger, L. J. Li, Y. K. Luo, G. H. Cao, Z. A. Xu, M. Loewenhaupt, J. P. Hu, and P. Dai, Phys. Rev. Lett. **102**, 107006 (2009).
[30] R. M. Fernandes, L. H. VanBebber, S. Bhattacharya, P. Chandra, V. Keppens, D. Mandrus, M. A. McGuire, B. C. Sales, A. S. Sefat, and J. Schmalian, Phys. Rev. Lett. **105**, 157003 (2010).
[31] P. Coleman and A. J. Schofield, Nature (London) **433**, 226 (2005).
[32] K. Haule and G. Kotliar, Phys. Rev. B **76**, 092503 (2007).
[33] A. V. Silhanek, N. Harrison, C. D. Batista, M. Jaime, A. Lacerda, H. Amitsuka, and J. A. Mydosh, Physica (Amsterdam) **378B–380B**, 373 (2006).

Supplementary material: Avoided quantum criticality and magnetoelastic coupling in $BaFe_{2-x}Ni_xAs_2$

PACS numbers: 74.70.Xa, 75.30.Gw, 78.70.Nx

Section A: **Details of the neutron and X-ray scattering experiments**

Neutron scattering experiments: The RITA-II uses a pyrolytic graphite (PG) filter before the sample and a cold Be filter after the sample with the final neutron energy fixed at $E_f = 4.6$ meV [1]. HB-1A spectrometer operates with a fixed incident neutron energy of $E_i = 14.64$ meV using a double PG monochromator. The second-order contamination in the beam was removed by placing two PG filters located before and after the second monochromator. A collimation of $48'$-$48'$-sample-$40'$-$68'$ from reactor to detector was used throughout the measurements. C5 uses PG as monochromator and analyzer with fixed $E_f = 14.56$ meV [2]. The sample orientation and setup are similar to those described previously [1]. Figure S1 shows the Ni-doping dependence of the incommensurate AF order. For $BaFe_{2-x}Ni_xAs_2$ samples with $x = 0.085, 0.092$, we see clear incommensurate static AF order below T_N.

X-ray diffraction experiments: The monochromator was Si(111) and incident beam energy was set at $E_i = 10$ keV with spot size of 1×1 mm^2 on the samples. In all cases, the data were collected on warming from base temperature to a temperature well above T_s.

Section B: **The proposed theoretical model:**

The proposed Landau–Ginzburg action is $S = S_M + S_{\rm lat} + S_{{\rm lat}-M}$. The magnetic part S_M (here $M_{A/B}$ refers to sublattice magnetization) is specified by

$$
\begin{aligned}
S_M &= \int d\{\mathbf{q}\} \int \mathbf{d}\{\omega\}[\mathbf{S_2}(\mathbf{q},\omega) + \mathbf{S_4}(\{\mathbf{q}\},\{\omega\}) + \ldots], \\
S_2(\mathbf{q},\omega) &= \sum_{\tau=A,B} \left(\alpha_m + c_M(\mathbf{q}-\mathbf{Q})^2 + \gamma|\omega|\right) \mathbf{M}_\tau^2 + (\cos q_x - \cos q_y)\mathbf{M}_A \cdot \mathbf{M}_B \\
S_4(\{\mathbf{q}\},\{\omega\}) &= u \sum_{\tau=A,B} |\mathbf{M}_\tau|^4 + u'|\mathbf{M}_A|^2 \, |\mathbf{M}_B|^{\,2} - v|\mathbf{M}_A \cdot \mathbf{M}_B|^2
\end{aligned}
$$

Here, S_2 describes the quadratic contribution of magnetic fluctuations, which includes a Landau damping γ [3]. The quartic term S_4 describes mode-mode interaction between magnetic fluctuations on the same and on different magnetic sublattices; the last term has a negative coefficient ($-v < 0$), favoring the collinear alignment of spins on the two sublattices [4]. There are also lattice parts:

$$
\begin{aligned}
S_{\rm lat} &= \int d\{\mathbf{q}\} \int d\{\omega\} \left(\alpha_s + c_s q^2 + \Gamma_s \frac{|\omega|}{q}\right) |\phi|^2 \\
&\quad + w \int d\{\mathbf{q}\} \int d\{\omega\} \, \phi^4 \\
S_{{\rm lat}-M} &= -\eta \int d\{\mathbf{q}\} \int d\{\omega\} \, (\mathbf{M}_A \cdot \mathbf{M}_B) \, \phi
\end{aligned}
$$

The last term describes magneto-elastic coupling, leading to an Ising magnetic order when the lattice orthorhombicity $\delta \equiv \langle\phi\rangle$ develops.

[1] H. Q. Luo, R. Zhang, M. Laver, Z. Yamani, M. Wang, X. Y. Lu, M. Y. Wang, Y. C. Chen, S. L. Li, S. Chang, J. W. Lynn, and P. Dai, Phys. Rev. Lett. **108**, 247002 (2012).

[2] H. Q. Luo, Z. Yamani, Y. C. Chen, X. Y. Lu, M. Wang, S. L. Li, T. A. Maier, S. Danilkin, D. T. Adroja, and P. Dai Phys. Rev. B **86**, 024508 (2012).

[3] J. A. Hertz, Phys. Rev. B **14**, 1165 (1976); A. J. Millis, Phys. Rev. B **48**, 7183 (1993).

[4] P. Chandra, P. Coleman, and A. I. Larkin, Phys. Rev. Lett. **64**, 88 (1990).

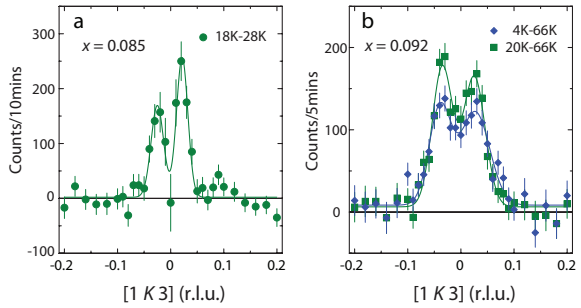

SFig 1: Ni-doping evolution of incommensurate magnetic peaks for (a) $x = 0.085$ and (b) $x = 0.092$ in $BaFe_{2-x}Ni_xAs_2$. The data are obtained carrying out scans along the $[1, K, 3]$ direction at different temperatuers. We obtain the net magnetic scattering at low temperatures by subtracting the high-temperature ($T > T_N$) background.